Journal of Solid State Chemistry 185 (2012) 89–94

Contents lists available at SciVerse ScienceDirect

Journal of Solid State Chemistry

journal homepage: www.elsevier.com/locate/jssc

Transition metal-chelating surfactant micelle templates for facile synthesis of mesoporous silica nanoparticles

Hye Sun Lee [a,b], Won Hee Kim [a], Jin Hyung Lee [a], Doo Jin Choi [b], Young-Keun Jeong [c], Jeong Ho Chang [a,*]

[a] Korea Institute of Ceramic Engineering and Technology, Seoul 153-801, Republic of Korea
[b] Department of Materials Science and Engineering, Yonsei University, Seoul 120-749, Republic of Korea
[c] National Core Research Center for Hybrid Materials Solution, Pusan National University, Pusan 609-735, Republic of Korea

ARTICLE INFO

Article history:
Received 1 July 2011
Received in revised form
28 September 2011
Accepted 23 October 2011
Available online 9 November 2011

Keywords:
Mesoporous silica nanoparticles
Metal-chelating surfactant
Micelle templates
Complex
Stability constant

ABSTRACT

Highly ordered mesoporous silica nanoparticles with tunable morphology and pore-size are prepared by the use of a transition metal-chelating surfactant micelle complex using Co^{2+}, Ni^{2+}, Cu^{2+}, and Zn^{2+} ions. These metal ions formed a metal-P123 micelle complex in an aqueous solution, while the metal ions are chelated to the hydrophilic domain such as the poly(ethylene oxide) group of a P123 surfactant. The different complexation abilities of the utilized transition metal ions play an important role in determining the formation of nano-sized ordered MSNs due to the different stabilization constant of the metal-P123 complex. Consequently, from a particle length of 1700 nm in the original mesoporous silica materials, the particle length of ordered MSNs through the metal-chelating P123 micelle templates can be reduced to a range of 180–800 nm. Furthermore, the variation of pore size shows a slight change from 8.8 to 6.6 nm. In particular, the Cu^{2+}-chelated MSNs show only decreased particle size to 180 nm. The stability constants for the metal-P123 complex are calculated on the basis of molar conductance measurements in order to elucidate the formation mechanism of MSNs by the metal-chelating P123 complex templates. In addition, solid-state ^{29}Si, ^{13}C-NMR and ICP-OES measurements are used for quantitative characterization reveal that the utilized metal ions affect only the formation of a metal-P123 complex in a micelle as a template.

1. Introduction

Remarkable research on the preparation of nano-sized ordered mesoporous silica (MS) materials has recently reported outcomes involving extremely high surface areas, large pore volumes, and tunable pore and particle sizes. One example is the MS nanoparticle (MSN) [1–16]. The MSN is a convenient reservoir because of its highly ordered porous structure. Several synthetic strategies have been used to control the size of MSNs [17–22]. Typical synthetic processes for controlling the particle morphology and surface properties of MSNs involve the use of an organic surfactant and a co-surfactant in a sol–gel reaction [23,24] as well as a high-speed centrifugation rate in excess of 13,000 rpm [25].

However, these processes suffer from the enhancement of production yields and the easy control of micelles. Furthermore, to date there have been no theoretical or mechanistic studies on facile MSNs preparation methods that are capable of high yields and size control.

Here, we propose a convenient method of preparing MSNs with size-tunable ordered meso-structures using the metal–chelating surfactant complex templates. Based on the concepts of silica chemistry, surfactant theory, and coordination chemistry, the proposed method involves the use of a metal-chelating surfactant complex as a mesostructure-directing agent. We synthesized highly ordered MSNs by adding transition metal salts such as Co^{2+}, Ni^{2+}, Cu^{2+}, and Zn^{2+} to a Pluronic P123 (P123, PEO_{20}–PPO_{70}–PEO_{20}) surfactant micellar solution. These metal ions form the metal-P123 micelle complex in an aqueous solution, and the utilized metal ions are chelated with the hydrophilic domain such as poly(ethylene oxide) fragments of the P123 surfactant. The different complexation degree of the metal ions plays an important role in determining the formation of nano-sized ordered MSNs due to the different stability constant for metal-P123 complexation. Our previous work reported that the ordered mesoporosity formation such as cores and walls are closely dependent on the control of the hydrophilic and hydrophobic domain of the surfactant micelles [26]. Furthermore, the addition of transition metal ions to form a metal–surfactant complex is crucial in the self-assembly of surfactant micelles to form the hexagonal packing with silicate species. Complete hydrolysis of a silica precursor under an acidic condition and a subsequent steady assembly of negative silicate species and positive metal ions effectively improve

* Corresponding author.
E-mail address: jhchang@kicet.re.kr (J.H. Chang).

0022-4596/$ - see front matter © 2011 Elsevier Inc. All rights reserved.
doi:10.1016/j.jssc.2011.10.037

highly ordered MSNs. Among the four transition metal ions used in this study, copper ion significantly affects the determination of the MSNs' particle-size. This new approach of metal-chelating surfactant micelle complex templates is useful and enables the synthesis of the nano-sized MSNs involving the accessible ordered pores in a wide variety of practical fields, such as nanoscopic reactors and containers. Moreover, this approach to the use of nano-sized materials in biomolecular separation has many immediate advantages over conventional micron-sized MSNs-based processes: for instance, it has higher production yields, higher surface-to-volume areas, enhanced binding rates, higher efficiency, and higher specificity.

2. Experimental

2.1. Preparation of transition metal-chelating P123 micelle templated MSNs

A metal-chelating micelle complex solution was prepared as follows. A Pluronic P123 micelle solution (4.0 g of Pluronic P123 in 30 g of water and 120 g of 2 M-HCl) was prepared at 40 °C and added to 5.0 M of a solution of transition metal salts, namely $CoCl_2 \cdot 6H_2O$, $NiCl_2 \cdot 6H_2O$, $CuCl_2 \cdot 6H_2O$, and $ZnCl_2 \cdot 6H_2O$. The mixture was stirred for 2 h and then supplemented with tetraethyl orthosilicate (TEOS, 8.5 g), after which it was aged in a stainless steel bomb at 120 °C overnight without stirring. The solid product was filtered, washed with excess water, and air-dried at room temperature. The calcination was carried out in air at 550 °C for 6 h.

2.2. Instrumental analyses

The obtained metal-chelating surfactant templated MSNs were structurally analyzed by means of instrumental analyses (namely, wide and small angle XRD, dynamic light scattered (DLS) particle-size distribution, and X-ray photoelectron spectroscopy (XPS)). The nitrogen adsorption and desorption isotherms were measured with a Quantachrome Autosorb-6 system. The pore size distributions were calculated from the analysis of the adsorption branch of the isotherm using the Barrett–Joyner–Halenda (BJH) method. The pore volume was taken at the five points of P/P_0. The XPS measurements were obtained with a SSI 2803-S spectrometer with a Al $K\alpha$. X-ray source of 12 kV and 20 mA. All core-level spectra were obtained at a photoelectron takeoff angle of 35° with respect to the sample surface. To compare the surface charging effect, all binding energies were referenced to a C 1*s* neutral carbon peak at 284.6 eV.

The small angle XRD patterns were taken with a Rigaku Denki instrument under conditions of 40 kV, and 160 mA Cu $K\alpha$ radiation. The scattered intensity was measured over the scattering vectors of $q=(4\pi/\lambda)\sin\theta$, where 2θ is the total scattering angle and λ is the wave length (Cu $K\alpha$ radiation, $\lambda=1.54$ Å); those values were generated from a rotating anode source monochromatized by means of a crystal monochrometer. The scattering curves were measured with a point focusing scintillation detector. The electron microscopic measurements, TEM, and SEM were taken with a JEOL JEM-4010 TEM (400 kV) and a JEOL JSM 6700F, respectively. Infra-red and ultraviolet-visible spectra were obtained from a JASCO V-460 and JASCO V-550. The techniques included an attenuated total reflectance Fourier transform IR technique and diffused reflectance ultraviolet-visible spectroscopy, respectively. Inductively coupled plasma-optical emission spectrometer (ICP-OES) titration was used to quantitatively determine the transition metal ions. For this process, we put a 0.1 g sample into a solution comprising 40 mL of 85%(w/w) phosphoric acid and 5 mL of a 1%(w/w) ammonium metavanadate solution in 0.9 M sulfuric acid; we then added 5 mL of 48%(w/w) hydrofluoric acid. The solution was kept in a water bath at 60 °C to dissolve the samples perfectly. Back-titration was achieved with 0.05 N of potassium dichromate to reduce the vanadate completely. The following equation gives the total amount of MO [27].

$$\%\mathrm{MO} = [N\mathrm{K_2Cr_2O_7}(V_{\mathrm{sample}} - V_{\mathrm{blank}}) \times 7.185]/m_{\mathrm{sample}}$$

where $N\mathrm{K_2Cr_2O_7}$ is the normality of potassium dichromate, V_{sample} and V_{blank} are the titrant volume of the sample and blank, respectively, and m_{sample} is the initial weight of the sample in grams.

3. Results and discussion

Fig. 1 shows schematic diagrams of the preparation of highly ordered MSNs with size-tunability by means of transition metal-chelating surfactant micelle templates. Although the synthetic route is similar to that of ordered mesoporous silica (SBA-15), which is prepared using non-ionic poly (ethyleneoxide)-poly(propyleneoxide)-poly(ethylene oxide) triblock copolymers. The utilization of

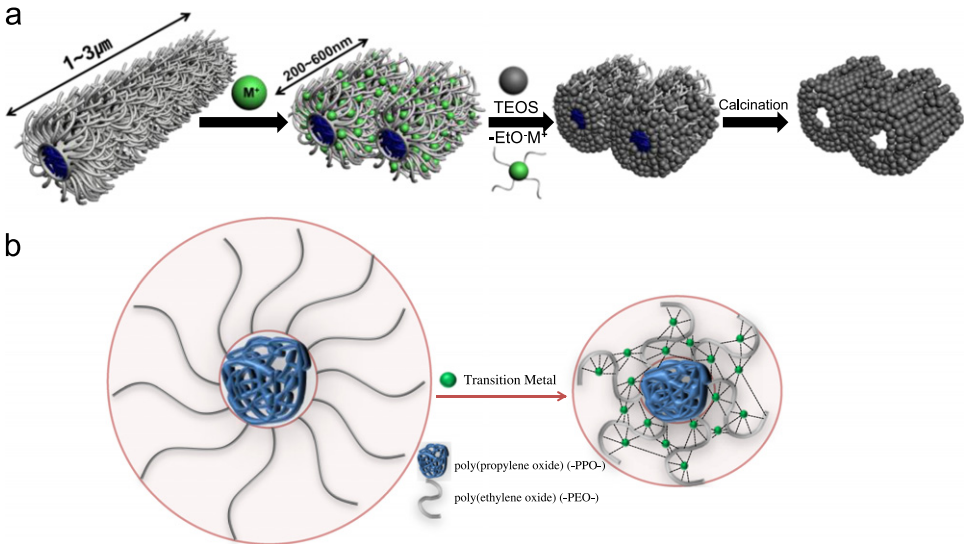

Fig. 1. (a) Schematic diagrams of the preparation of MSNs by a transition metal-chelating P123 micelle template and (b) comparison of micelle size between natural P123 micelle and the Cu^{2+}-chelated P123 micelle complex.

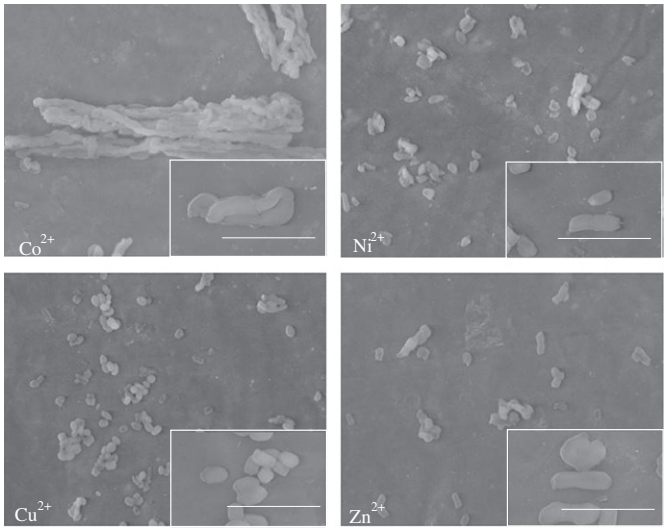

Fig. 2. SEM images of transition metal-chelating MSNs through the metal-chelating P123 micelle templates. (The scale bars in SEM images are 100 nm).

metal-chelating surfactant micelle, M^{n+}–P123 complex, is a unique process to control the MSNs particle size. Based on the measurement of particle size distribution by the dynamic light scattering (DLS) method, the natural P123 micelle (metal ion free) exhibits a 300 nm particle size in an aqueous solution, but metal-chelating P123 micelle shows a 25 nm particle size. This result is attributed to the complexation between poly(ethylene oxide) fragments of P123 and metal ions (Fig. 1(b)).

Fig. 2 shows the SEM and TEM images of obtained MSNs after calcination through the metal-chelating P123 surfactant templates. SEM images of typical MS have an aspect ratio in the range of 3.3–10, particle lengths of 1–3 μm, and particle diameters of 200–300 nm. However, SEM images of MSNs through transition metal-chelating templates shows the decreased aspect ratios of 3.2, 2.5, 1.3, and 2.1 for the Co^{2+}, Ni^{2+}, Cu^{2+}, and Zn^{2+} complex templates, respectively, while the particle lengths are tunable in the range of 800–180 nm. In particular, the Cu^{2+}-chelated MSNs only have an aspect ratio of 1.3 and a particle length of 180 nm. The TEM images show the pores and channels are of uniform size and exhibit a hexagonal array of lattice fringes as well as parallel fringes that correspond to a side-on view of the pores (Fig. S-1(c) in Supplementary materials). Remarkably, the obtained MSNs through transition metal-chelating templates have a pore size of 6.60 nm ± 3 nm for all used transition metal ions whereas MS itself has a pore size of 8.48 nm. The slight discrepancy of 1.86 nm is attributed to the complex formation of the metal-poly(propylene oxide) fragments in the hydrophobic region as a PPO core. However, the subsequent increase in wall-thickness tends to induce a decrease in pore size due to an increase in the reaction domain with TEOS and the metal-P123 micelle complex. For example, original MS has a pore size of 8.48 nm and a wall thickness of 6.60 nm, whereas the Cu^{2+}-chelating MSNs have a pore size of 6.62 nm and a wall thickness of 8.77 nm. Changes in the pore size are unlikely to occur if a non-ethylene oxide block co-polymer such as polystyrene is used because the absence of oxygen prevents any coordinated bonding of the metal-surfactant complex.

Fig. 3 shows the detailed characterization of the obtained MSNs through transition metal-chelating templates by small angle XRD, X-ray photoelectron spectroscopy (XPS), and particle size distribution with a dynamic light scattering method. The small angle XRD patterns of metal-chelating micelle templated MSNs show the main diffraction patterns at 0.85, 1.63, and 1.82 of 2θ degrees for (100), (110), and (200), respectively, in which these diffraction patterns are similar to the original MS (Fig. 3(a)). However, the diffraction patterns of Cu^{2+} and Zn^{2+} are slightly smaller than the 2θ degrees of the original MS diffraction. This difference is attributed to the pore-confinement effect; that is, a small amount of metal chelation occurs in a hydrophobic domain of P123P123, such as a PPO fragment in a micellar core, and the pore size of the MSNs is consequently smaller than that of MS. XPS measurement is conducted for a quantitative analysis of Si and O elements as a function of transition metal complex templates (Fig. 3(b)). The spectrum shows that the main element of Si and O electronic configuration peaks are detected at 149 eV, 100 eV, and 520 eV for Si_{2s}, Si_{2p}, and O_{1s}, respectively. The XPS spectra of the metal-chelating MSNs do not reflect any transition metal peaks. These results are in good agreement with those of an inductively coupled plasma optical emission spectrometer (ICP-OES). To enhance the accuracy of the particle size analysis, we measure the particles with a dynamic light scattering method (Fig. 3(c)). The results reveal that the average particle size is 1650 nm for typical MS, and 180 nm for the Cu^{2+}-chelating MSNs. Furthermore, a comparison of the micelle size of pure P123 and Cu^{2+}-chelating P123 shows that the average micelle size is 300 nm for typical MS and 13 nm for Cu^{2+}-chelating MSNs (Fig. 3(d)).

Table 1 shows the N_2 adsorption Bruauner–Emmet–Teller (BET) parameters such as pore sizes and pore volumes, including the particle size distribution of metal-chelating templated MSNs as a function of various kinds of metal ions. The particle size distribution of the obtained MSNs shows reduced lengths of 850 nm, 550 nm, 180 nm, and 700 nm for the Co^{2+}, Ni^{2+}, Cu^{2+}, and Zn^{2+}–P123 complex templates, respectively. Although the conventional preparation of MSNs has the disadvantage of a small pore size of less than 3 nm due to the difficult control of small micelles [23,24], our approach provides little change in the pore size distribution from 8.8 nm to 6.62 nm due to interaction with the hydrophilic shell (PEO regions) of the P123 micelles. Moreover, BET isotherms of the obtained MSNs have the hysteresis loop pattern of the H4 type, which confirms that the metal-chelating MSNs retain their pore size (Fig. S1(a)). The pore volumes of the MSNs of the metal-P123 complexes are 0.91 mL/g, 0.93 mL/g, 0.96 mL/g, and 0.88 mL/g for the Co^{2+}, Ni^{2+}, Cu^{2+}, and Zn^{2+}–P123 complex templates, respectively. Among the four metal species, the Cu^{2+}-chelating MSNs have the largest pore volume, 0.96 mL/g. In contrast, the pore volume of MS is 1.06 mL/g.

To elucidate the Cu^{2+} chelation effect on the formation of metal-chelating templated MSNs, we applied the solid-state ^{13}C NMR technique. We acquired solid-state ^{13}C NMR spectra for the pure surfactant (P123) and the final solid precipitate, mesoporous silica materials, (Cu^{2+}/P123/silicate) [28–30]. The spectra have two peaks associated with a hydrophilic region (PEO) and a hydrophobic region (PPO) near 75 ppm and 17 ppm, respectively (Fig. 4(a)). The feature attributed to the hydrophilic region by the Cu^{2+} chelation in the P123/silicate material shows an intensity change in the shape of the peak, which differs from the peak of the pure P123. This change in the peak is likely due to the interaction between PEO and Cu^{2+} ions. The hydrophobic peak (PPO) at 17 ppm for the P123/silicate material has a downfield shift of approximately 2 ppm and is narrower than that of the pure P123. This outcome, which may be attributed to the pore confinement effect from the reduced mobility, is confirmed by the relaxation time measurement and the residual interaction between the oxygen in PPO and the Cu^{2+} ions. Furthermore, single-pulse ^{29}Si NMR spectra were obtained via long recycle times (30 s) of a Bloch decay-pulse with single-pulse excitation (Fig. 4(b)). The initial ^{29}Si NMR spectra of the MS were at −97 ppm, −104 ppm, and −113 ppm for the $(HO)_2Si(OSi)_2$ (Q^2), $HOSi(OSi)_3$ (Q^3), and $Si(OSi)_4$

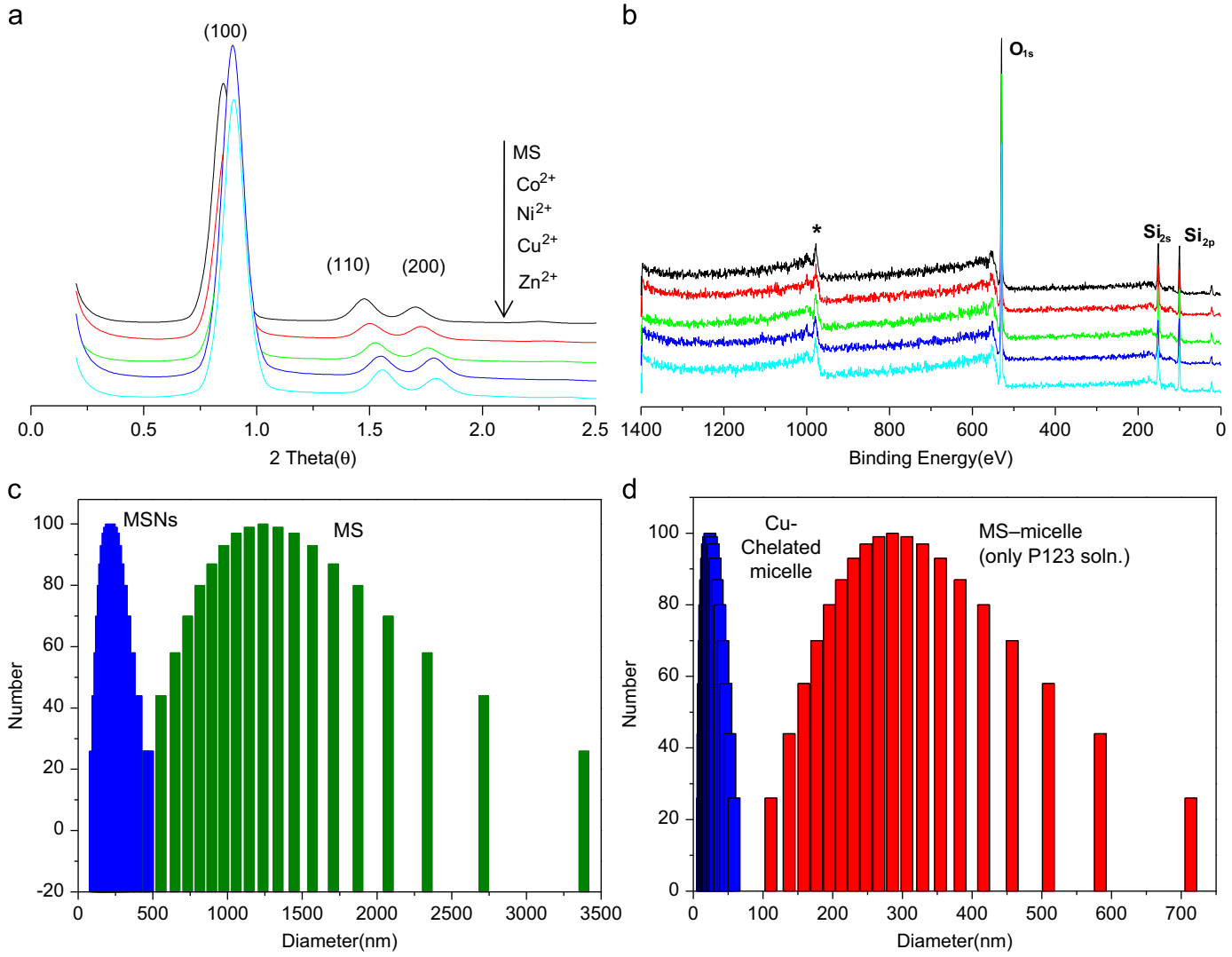

Fig. 3. (a) Small-angle XRD patterns, (b) XPS spectrum as a function of transition metal-chelating MSNs, (c) comparison of the particle size distribution of MS and Cu^{2+}-chelating MSNs and (d) comparison of micelle size of Cu^{2+}–P123 complex and Cu^{2+}-free micelle as determined by a dynamic light scattering (DLS) method.

Table 1
Comparison of BET parameters and particle size distribution of metal-chelating templated MSNs as a function of added transition metal ions.

Samples	Pore size (nm)[a]	Wall thickness (nm)[b]	S_{BET} (m^2/g)	Pore volume (mL/g)	Particle size (nm)[c]
MS	8.80	2.84	758	1.06	1650
MSN-Co	6.62	4.81	608	0.91	850
MSN-Ni	6.62	5.37	636	0.93	550
MSN-Cu	6.62	5.37	700	0.96	180
MSN-Zn	6.62	5.39	615	0.88	700

[a] Pore size.
[b] Wall thickness.
[c] Particles size distribution were obtained by BET, small angle XRD, and DLS, respectively.

(Q^4) silicate species, respectively, where Q^n represents silicon atoms bonded to n neighboring silicon atoms via Si–O–Si bonds [31–34]. The high Q^3 and Q^4 peaks represent the high surface areas and wall thickness of typical MS. After the metal chelation, the metal-chelating MSNs show a significant increase in the Q^4 peak, such as the $-(OSi)_4$ segments, due to the increase in wall thickness. The ratio of the relative peak areas of the Q^4 over Q^3 signals is 0.24 for MS, and 1.08 for metal-chelating MSNs. These increased ratios reveal that the gap between each mesoporous micelle in the metal-chelating MSNs is wide due to the dispersion by metal chelation (see the inset diagrams a′ and b′). In addition, we achieved the conductance measurements to calculate the stability constant (K) for the complexation between the transition-metal ions and P123P123 surfactant. The stability constants, which are determined by the molar conductance (Λ) measurement in the presence of polymeric ligand with metal ions, are a quantitative characteristic in the formation of the metal-P123 complex. The complex formation of polymers with metals differs from similar processes involving a low molecular weight ligand because the microenvironment of the corresponding binding groups of the polymer changes as the complex formation proceeds. The calculation of stability constant (K) for these complexes is calculated by consecutive approximations from the following equation [35,36]:

$$(\Lambda_A-\Lambda)/[P123]_e = K(\Lambda-\Lambda_B)$$

where $[P123]e=[P123]_0-[M]^+$ $(\Lambda_A-\Lambda)/(\Lambda-\Lambda_B)$ is the equilibrium concentration of P123 at 25 °C, Λ_A is the equivalent conductance of the transition metal, and Λ_B is the normalized equivalent conductance of the complex as an infinite quantity. From the plot of $(\Lambda_A-\Lambda)/[P123]_e$ vs. $(\Lambda-\Lambda_B)$, we can determine that the stability constants (log K) are 1.8, 2.4, 3.1, and 2.8 for the Co^{2+}, Ni^{2+}, Cu^{2+}, and Zn^{2+} complexes, respectively (Fig. 5(a)). The detailed calculation

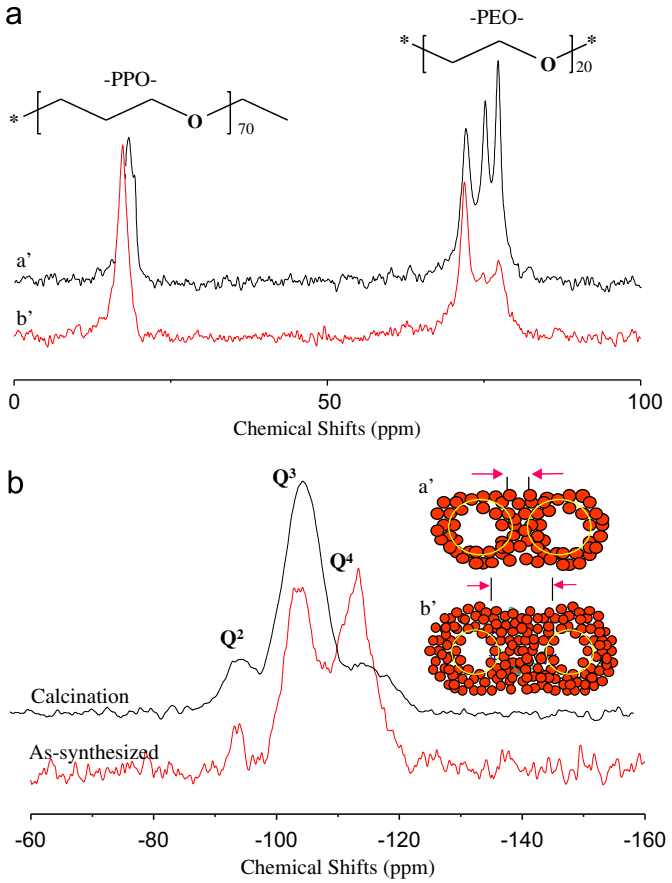

Fig. 4. (a) Solid-state ^{13}C-NMR spectra of (a′) MS and (b′) Cu^{2+}-chelating templated MSNs, (b) ^{29}Sii-NMR spectra of (a′) as-synthesized MS, and (b′) Cu^{2+}-chelating templated MSNs after calcination.

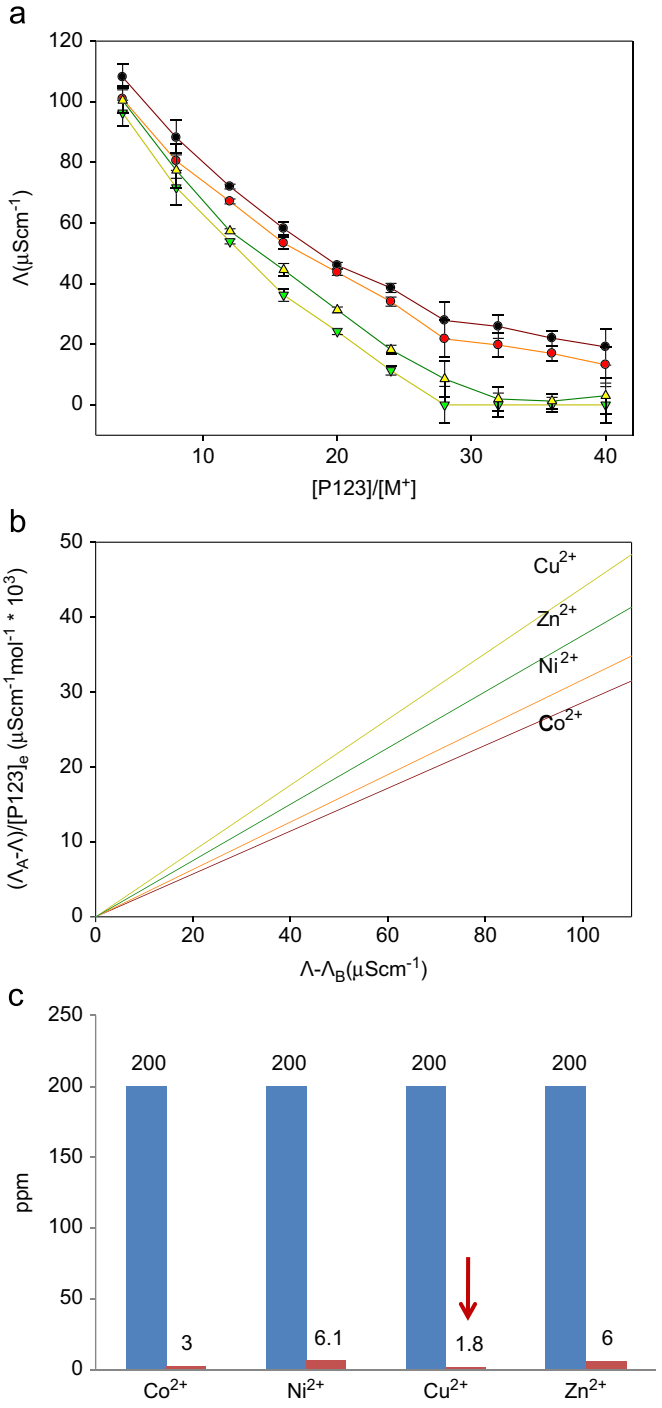

Fig. 5. (a) Plot of $(\Lambda_A-\Lambda)/[P123]_e$ vs. $(\Lambda-\Lambda_B)$, which is used to calculate the stability constant from the molar conductance (Λ) measurement of a metal-P123 complex, (b) the molar conductance (Λ) measurement of the metal-P123 complex as a function of the [P123] molar ratios and (c) quantitative analysis of the transition metal species in metal-chelating MSNs before and after calcination by ICP-OES titration.

for the Cu^{2+}-chelating template is shown in Table S1. The results coincide well with the Irving–Williams order of $Co^{2+} < Ni^{2+} < Cu^{2+} > Zn^{2+}$, where the Cu^{2+} ion has the largest K because of its higher radius and stability [37]. We also examined how the molar conductance (Λ) varies in relation to the molar ratio of the polymeric P123 ligand to the metal cations, [P123P123]/[M], for complexation at 25 °C (Fig. 5(b)). The plots show that the molar conductance decreases as the P123 concentration increases. This relation is due to the fact that the P123-metal complex has lower mobility than free metal ions. The results also imply that the degree of complexation in the P123-metal complex is not very strong because P123 has a long chain structure. Moreover, to elucidate the metal chelation effect on the formation of MSNs, we demonstrate the quantification of metal elements in MSNs before and after calcinations. For this purpose, we use an inductively coupled plasma optical emission spectrometer (ICP-OES) with an axial viewing configuration. The metal concentration of all the MSNs before calcination is 200 ppm as a detection limit, though the metal concentrations after calcination are changed to 3 ppm, 6.1 ppm, 1.8 ppm, and 6 ppm for the Co^{2+}, Ni^{2+}, Cu^{2+}, and Zn^{2+} complexes, respectively. Furthermore, there is no cross-linking with the silica matrix as a template if the use of transition metal ions in the formation of MSNs is caused solely by a strong chelation effect, which forms the metal-P123 complexes in the micelles.

4. Conclusion

We propose a simple and facile process of preparing size-tunable ordered MSNs. The process involves the use of transition metal-chelating surfactant micelle complex templates in high homogeneity. Conventional processes have difficulty in controlling surfactant micelles; however, the metal-chelating surfactant micelle complex templates can be reasonably applied to the self-rearrangement of metal-surfactant complex micelles for the formation of replicated small MSNs in a silica framework through the co-hydrolysis of TEOS and their proper precursors. Consequently, the MSNs through the metal-chelating surfactant micelle complex templates have a particle size in the range of 180–800 nm,

which is considerably smaller than the 1700 nm particles of MS, and the pores of the MSNs remain larger by 6.6 nm. The stability constants were calculated using the molar conductance measurement of metal-P123 complexes to elucidate the formation mechanism of metal-chelating templated MSNs. Furthermore, the solid-state ^{13}C-NMR and ICP-OES measurements for the quantitative characterization reveal that the metal ions are only involved in the formation of the metal-P123 complex in the micelles as a template. This preliminary study enables the facile design and construction of MSNs including nanoparticles and nanorods and overcomes the disadvantages of the conventional process, particularly the low yields and difficult synthetic process.

Acknowledgments

This work was supported by a grant from the Fundmental R&D Program for Core Technology of Materials funded by the Ministry of Knowledge Economy, Republic of Korea.

Appendix A. Supporting materials

Supplementary data associated with this article can be found in the online version at doi:10.1016/j.jssc.2011.10.037.

References

[1] X. Huang, X. Teng, D. Chen, F. Tang, J. He, Biomaterials 31 (2010) 438.
[2] F. Lu, S.H. Wu, Y. Hung, C.Y. Mou, Small 5 (2009) 1408.
[3] F. Gao, P. Botella, A. Corma, J. Blesa, L. Dong, J. Phys. Chem. B113 (2009) 1796.
[4] T. Xia, M. Kovochich, M. Liong, H. Meng, S. Kabehie, S. George, J.I. Zink, A.E. Nel, ACS Nano 3 (2009) 3273.
[5] C.P. Tsai, C.Y. Chen, Y. Hung, F.H. Chang, C.Y. Mou, J. Mater. Chem. 19 (2009) 5737.
[6] A.M. Chen, M. Zhang, D. Wei, D. Stueber, O. Taratula, T. Minko, H. He, Small 5 (2009) 2673.
[7] D.M. Huang, T.H. Chung, Y. Hung, F. Lu, S.H. Wu, C.Y. Mou, M. Yao, Y.C. Chen, Toxicol. Apply. Pharm. 231 (2008) 208.
[8] C.H. Lee, L.W. Lo, C.Y. Mou, C.S. Yang, Adv. Funct. Mater. 18 (2008) 3283.
[9] J. Lu, M. Liong, J.I. Zink, F. Tamanoi, Small 3 (2007) 1341.
[10] Y.F. Han, F. Chen, Z. Zhong, K. Ramesh, L. Chen, E. Widjaja, J. Phys. Chem. B110 (2006) 24450.
[11] J. Ren, J. Ding, K.Y. Chan, H. Wang, Chem. Mater. 19 (2007) 2786.
[12] H. Vallhov, S. Gabrielsson, M. Stromme, A. Scheynius, A.E. Garcia-Bennett, Nano Lett. 7 (2007) 3576.
[13] I.Y. Park, I.Y. Kim, M.K. Yoo, Y.J. Choi, M.H. Cho, C.S. Cho, Int. J. Pharm. 359 (2008) 280.
[14] J. Lu, M. Liong, S. Sherman, T. Xia, M. Kovochich, A.E. Nel, J.I. Zink, F. Tamanoi, Nanobiotechnology 3 (2007) 89.
[15] S. Gago, J.A. Fernandes, J.P. Rainho, R.A. Sa Ferreira, M. Pillinger, A.A. Valente, T.M. Santos, L.D. Carlos, P.J.A. Ribeiro-Claro, I.S. Goncalves, Chem. Mater. 17 (2005) 5077.
[16] Y.D. Wang, C.L. Ma, X.D. Sun, H.D. Li, Inorg. Chem. Commun. 5 (2002) 751.
[17] F. Torney, B.G. Trewyn, V.S.Y. Lin, K. Wang, Nat. Nanotech. 2 (2007) 295.
[18] Y. Lin, C.L. Haynes, J. Am. Chem. Soc. 132 (2010) 4834.
[19] H.P. Lin, C.Y. Mou, Acc. Chem. Res. 35 (2002) 927.
[20] J. Kim, H.S. Kim, N. Lee, T. Kim, H. Kim, T. Yu, I.C. Song, W.K. Moon, T. Hyeon, Angew. Chem. Int. Ed. 47 (2008) 8438.
[21] Y. Fing, D. Gu, Y. Zou, Z. Wu, F. Li, R. Che, Y. Deng, B. Tu, D.A. Zhao, Angew. Chem. Int. Ed. 49 (2010) 7987.
[22] A. Sayari, B. Han, Y. Yang, J. Am. Chem. Soc. 126 (2004) 14348.
[23] B.G. Trewyn, S. Giri, I.I. Slowing, V.S.Y. Lin, Chem. Commun. (2007) 3236.
[24] B.G. Trewyn, I.I. Slowing, S. Giri, H. Chen, V.S.Y. Lin, Acc. Chem. Res. 40 (2007) 846.
[25] K. Suzuki, K. Ikari, H. Imai, J. Am. Chem. Soc. 126 (2004) 462.
[26] J.H. Chang, L.Q. Wang, Y. Shin, B. Jeong, J.C. Birnbaum, G.J. Exarhos, Adv. Mater. 14 (2002) 378.
[27] F. Jiao, A. Harrison, A. Berko, V. Chadwick, P.G. Burh, J. Am. Chem. Soc. 128 (2006) 5468.
[28] B. Grünberg, T. Emmler, E. Gedat, I. Shenderovich, G.H. Findenegg, H.H. Limbach, G. Buntkowsky, Chem. Eur. J. 10 (2004) 5689.
[29] E. Gedat, A. Schreiber, J. Albrecht, T. Emmler, I. Shenderovich, G.H. Findenegg, H.H. Limbach, G. Buntkowsky, J. Phys. Chem. B106 (2002) 1977.
[30] Y. Komori, S. Hayashi, Micropor. Mesopor. Mater. 68 (2004) 111.
[31] N. Baccile, F. Babonneau, Micropor. Mesopor. Mater. 110 (2008) 534.
[32] A. Vyalikh, T. Emmler, I. Shenderovich, Y. Zeng, G.H. Findenegg, G. Buntkowsky, Phys. Chem. Chem. Phys. 9 (2007) 2249.
[33] J. Trébosc, J.W. Wiench, S. Huh, V.S.Y. Lin, M. Pruski, J. Am. Chem. Soc. 127 (2005) 3057.
[34] J. Trébosc, J.W. Wiench, S. Huh, V.S.Y. Lin, M. Pruski, J. Am. Chem. Soc. 127 (2005) 7587.
[35] E. Shchori, J. Jagur-Grodzinski, Z. Luz, M. Shporer, J. Am. Chem. Soc. 93 (1971) 7133.
[36] S.S. Mamedova, S.R. Gadzhieva, T.G. Khanlarov, Russ. J. Inorg. Chem. 53 (2008) 1964.
[37] J.E. Huheey, Inorganic Chemistry, Principles of Structure and Reactivity, 4th Ed., Harpercollins, New York, 1993 Chapter 8.